

Supporting Information

Bi-functional S-scheme cobalt-porphyrin conjugated polymer/C₃N₄ heterojunction for cooperative CO₂ reduction and tetracycline degradation

Chao Xu,^a Shien Guo,^{b*} Jiaxin Wang,^a Yiqing Jiang,^a Xiaomin Wu,^a Dandan Lin,^a
Yuting Xiao^{a*}

^aKey Laboratory of Jiangxi Province for Persistent Pollutants Prevention Control and Resources Reuse, Nanchang Hangkong University, Nanchang 330063, Republic of China.

^bSchool of Chemical Engineering, Jiangxi Normal University, Nanchang 330022, People's Republic of China.

Corresponding authors:

Yuting Xiao, Ph.D., Email: yutingxiao9@sina.com

Shien Guo, Ph.D., Email: guoshien@jxnu.edu.cn

Contents

Characterization	S3
Photoelectrochemical test	S3
Fig. S1. TEM image of CN nanosheets.	S6
Fig. S2. TEM image of CoPor-DBE nanoflakes.....	S6
Fig. S3. AFM image (a) and corresponding height profile (b) along the white of the 50CoPor-DBE/CN heterojunction	S7
Fig. S4. ¹³ C CP-MAS NMR spectra of Por-DBE.	S7
Fig. S5. N ₂ adsorption-desorption isotherms (inset pore-size distribution profile) of (a) CoPor-DBE, (b) CN, and (c) 50CoPor-DBE/CN composite.	S8
Table S1. The specific surface area and porosity of different samples.	S8
Fig. S6. Schematic diagram illustrating the S-scheme charge-transfer process in the CoPor-DBE/CN heterojunction.	S9
Fig. S7. DMPO spin-trapping ESR spectra recorded for (a) •O ₂ ⁻ and (b) •OH over CoPor-DBE, CN, and 50CoPor-DBE/CN.	S9
Fig. S8. Schematic diagrams of experimental setup for photocatalytic performance test.	S10
Table S2. Comparison of the activity of 50CoPor-DBE/CN in the cooperative CO ₂ reduction and tetracycline decomposition with the catalysts reported in literature...S11	S11
Fig. S7. (a) XRD pattern and (b) FT-IR spectra of 50CoPor-DBE/CN hybrid before and after cycling reaction.....	S13
Fig. S10. High-resolution Co 2p spectra of CoPor-DBE/CN before and after cycling test.	S13
Fig. S11. In-situ FT-IR measurements for CO ₂ photoreduction over 50CoPor-DBE/CN at room temperature under light irradiation.	S14
Table S3. Fitted parameters from time-resolved PL spectra of pristine CN, CoPor-DBE and 50CoPor-DBE/CN.....	S14

Characterization

Tetramethylsilane (TMS) as the internal standard, hydrogen nuclear magnetic resonance (NMR) spectra at 500 MHz and ^{13}C nuclear magnetic resonance (^{13}C NMR) spectra at 100 MHz or 150 MHz were acquired on a Bruker Avance spectrometer. Solid-state ^{13}C NMR spectra were recorded using a Bruker Avance III 500 and MAS III equipment. The specific surface area was determined using the Brunauer-Emmett-Teller (BET) method. The nitrogen adsorption-desorption isotherm was measured on a Micromeritics ASAP 2010 analyzer at a temperature of 77 K, following vacuum activation of the sample at 120 °C overnight prior to measurement. The powder X-ray diffraction (XRD) was recorded on a D8 Advance diffractometer with Cu K α radiation ($\lambda=0.15418$ nm) in the 2θ range from 2~60°. The morphology and microstructure was observed by transmission electron microscopy (TEM, Tecnai G2 F20). The UV-vis diffuse reflectance spectra (DRS) were measured on a Varian Cary 5000 UV-vis spectrophotometer with pure white BaSO $_4$ as the reference. X-ray photoelectron spectroscopy (XPS) and ultraviolet photoelectron spectroscopy (UPS) measurements were analyzed using an ESCA-Lab-200i-XL spectrometer (PHI, USA) with monochromatic Al K α radiation (1486.6 eV). Fourier transformation infrared spectra were recorded on a Nicolet 6700 (ThermoFisher, USA). Samples were dried and compressed to a plate with KBr for measurement. Steady-state photoluminescence (PL) spectra were collected by a FluoroMax-4 spectrofluorometer (Horiba Scientific). The time-resolved fluorescence decay spectra were measured by FLS980 spectrometer (Edinburgh Instruments, UK). Kelvin probe force microscope (KPFM) analysis was performed on a Multi Mode 8 Bruker spectrometer

Photoelectrochemical test

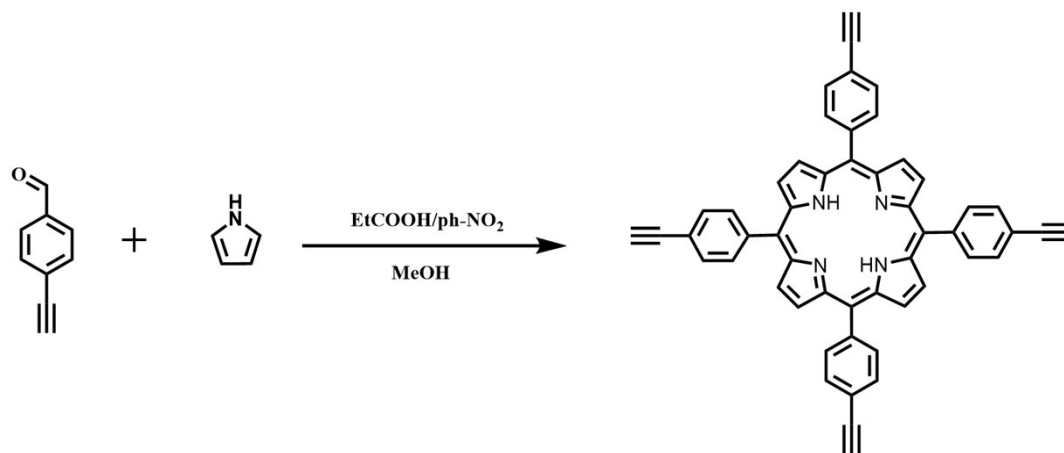
Photocurrent, Mott-Schottky plots, and electrochemical impedance spectroscopy were conducted using a standard three-electrode system on a CHI660E electrochemical workstation (Chenhua, China). The photocatalyst-coated FTO served as the working electrode, while platinum foil was utilized as the counter electrode, and an Ag/AgCl electrode was employed as the reference electrode. The working electrode was prepared

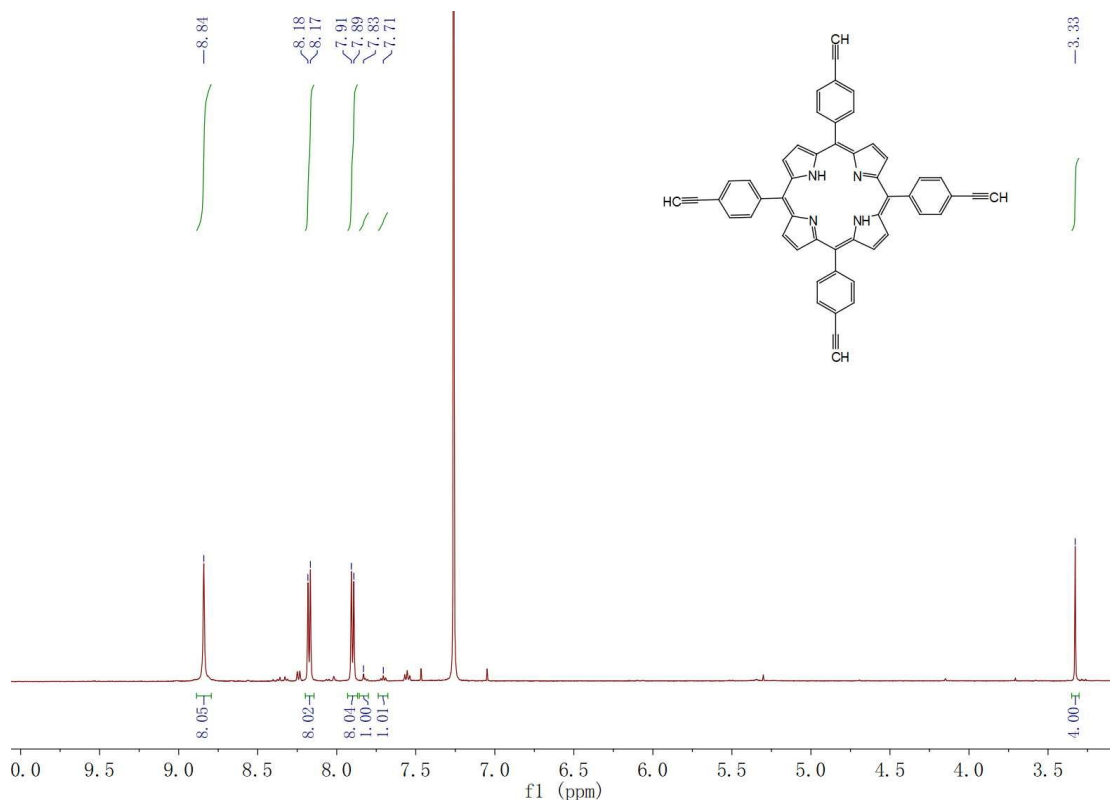
by applying a polymer aqueous slurry onto an FTO glass substrate with an area of 1 cm².

Synthesis of 5,10,15,20-tetrakis(4-ethynylphenyl) porphyrin

To a 250 ml round bottom flask was added 4-ethynylbenzaldehyde (2.6 g, 20 mmol), 60 ml of propionic acid, 30 ml of nitrobenzene, sonicated to dissolve 4-ethynylbenzaldehyde. The reaction was heated to 140 °C. 1.4 ml of pyrrole was added slowly using a constant pressure dispensing funnel and the reaction was allowed to run for 90 minutes, then the system was cooled to 60 °C. The reaction was stopped by the addition of 10 ml of methanol and stirring for half an hour. The product was filtered and washed with methanol. After vacuum drying, 1.0g of purple powder Por (5,10,15,20-tetrakis(4-ethynylphenyl) porphyrin) was obtained in 27.9% yield.

¹H NMR (500 MHz, Chloroform-*d*) δ 3.30 – 3.35 (s, 4H), 7.68 – 7.74 (t, *J* = 7.2 Hz, 1H), 7.80 – 7.86 (d, *J* = 5.9 Hz, 1H), 7.87 – 7.93 (d, *J* = 7.7 Hz, 8H), 8.14 – 8.20 (d, *J* = 7.7 Hz, 8H), 8.79 – 8.89 (s, 8H)

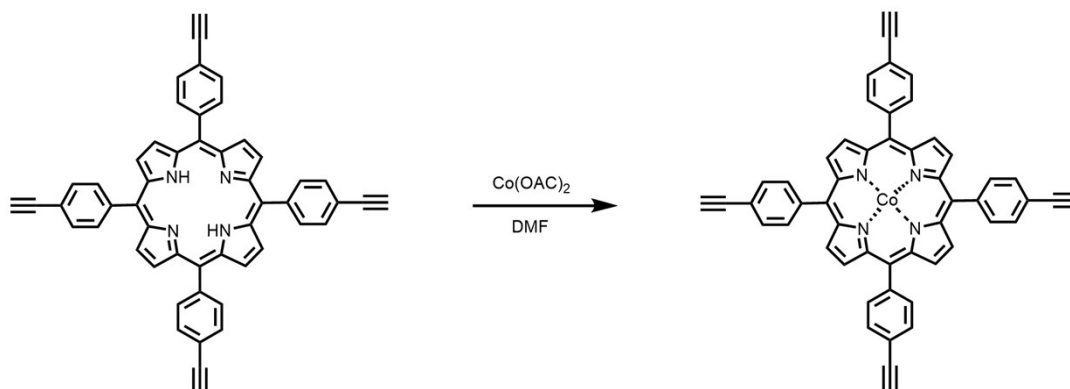




¹H NMR spectra of Por in DMSO-d₆.

Synthesis of Co(II)-5,10,15,20-tetrakis(4-ethynylphenyl) porphyrin

To a 100 ml round bottom flask was added Por (290.4 mg, 0.4 mmol), anhydrous cobalt acetate (141.2 mg, 0.8 mmol) and 60 ml of DMF and reacted under argon at 140°C for 4 hours. The crude product was extracted with water and dichloromethane to remove DMF and evaporated under reduced pressure to give a brown-red solid. The resulting product was dissolved with ethyl acetate, filtered to remove the solid, and the ethyl acetate was evaporated under reduced pressure to give Co-Por (Co(II)-5,10,15,20-tetrakis(4-ethynylphenyl)porphyrin).



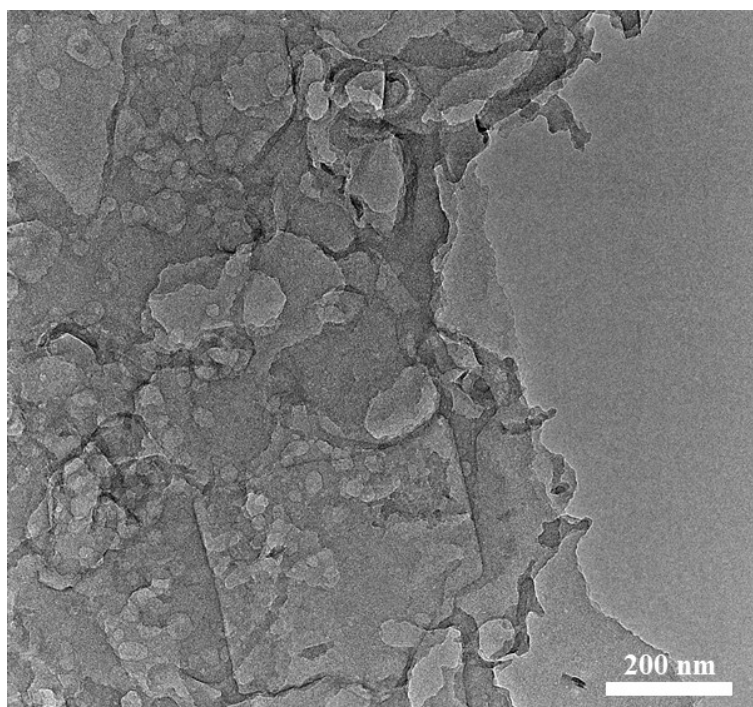


Fig. S1. TEM image of CN nanosheets.

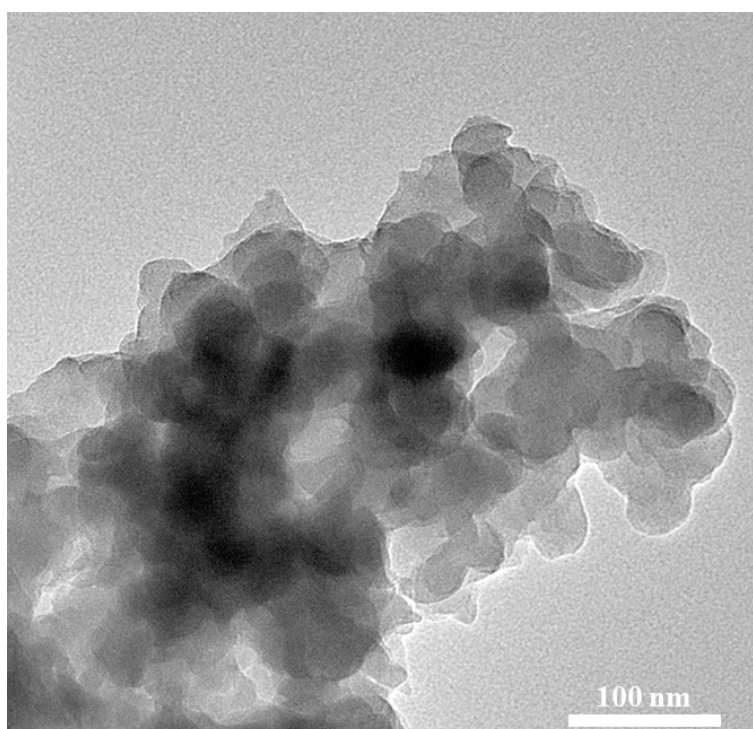


Fig. S2. TEM image of CoPor-DBE nanoflakes.

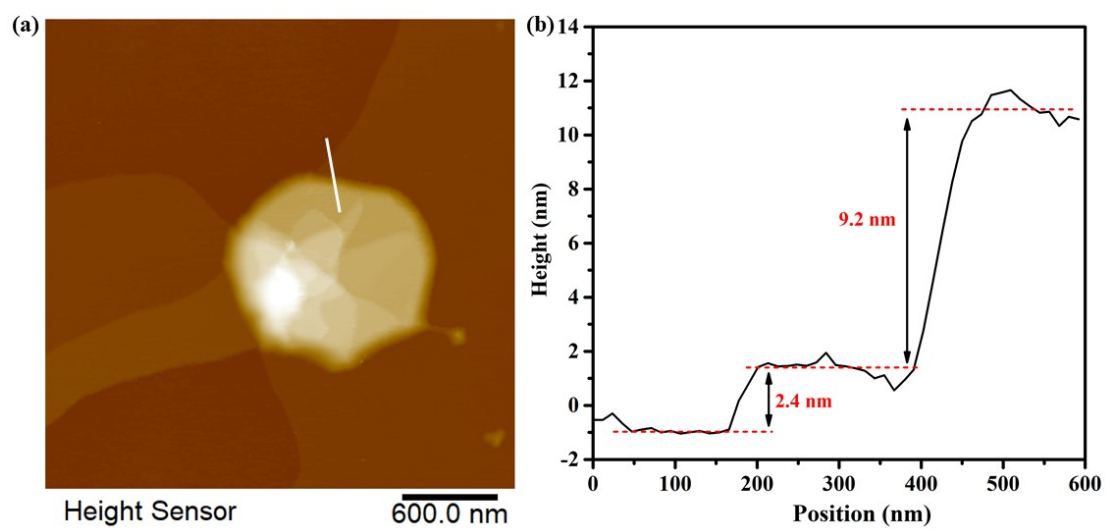


Fig. S3. AFM image (a) and corresponding height profile (b) along the white of the 50CoPor-DBE/CN heterojunction

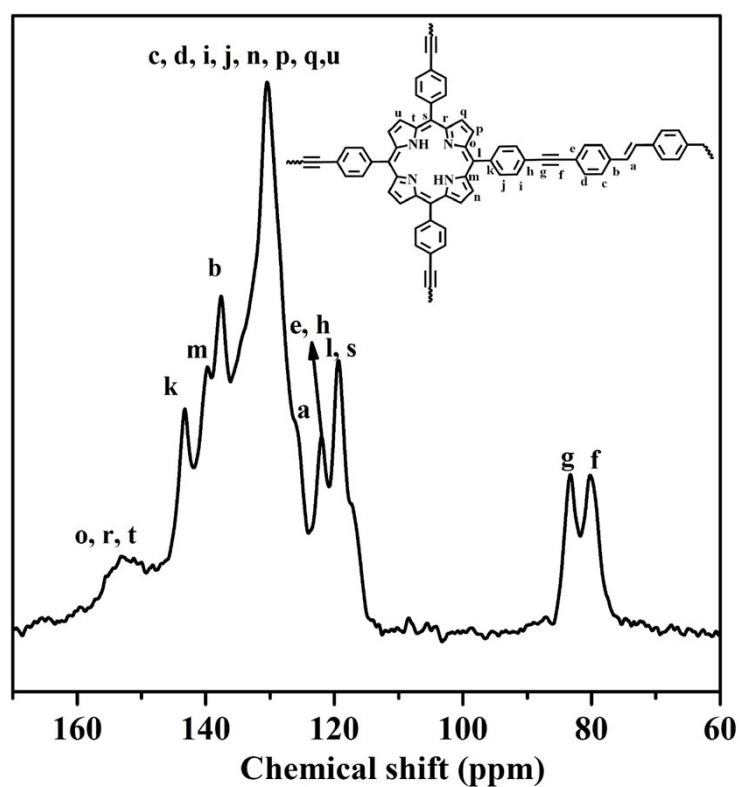


Fig. S4. ¹³C CP-MAS NMR spectra of Por-DBE.

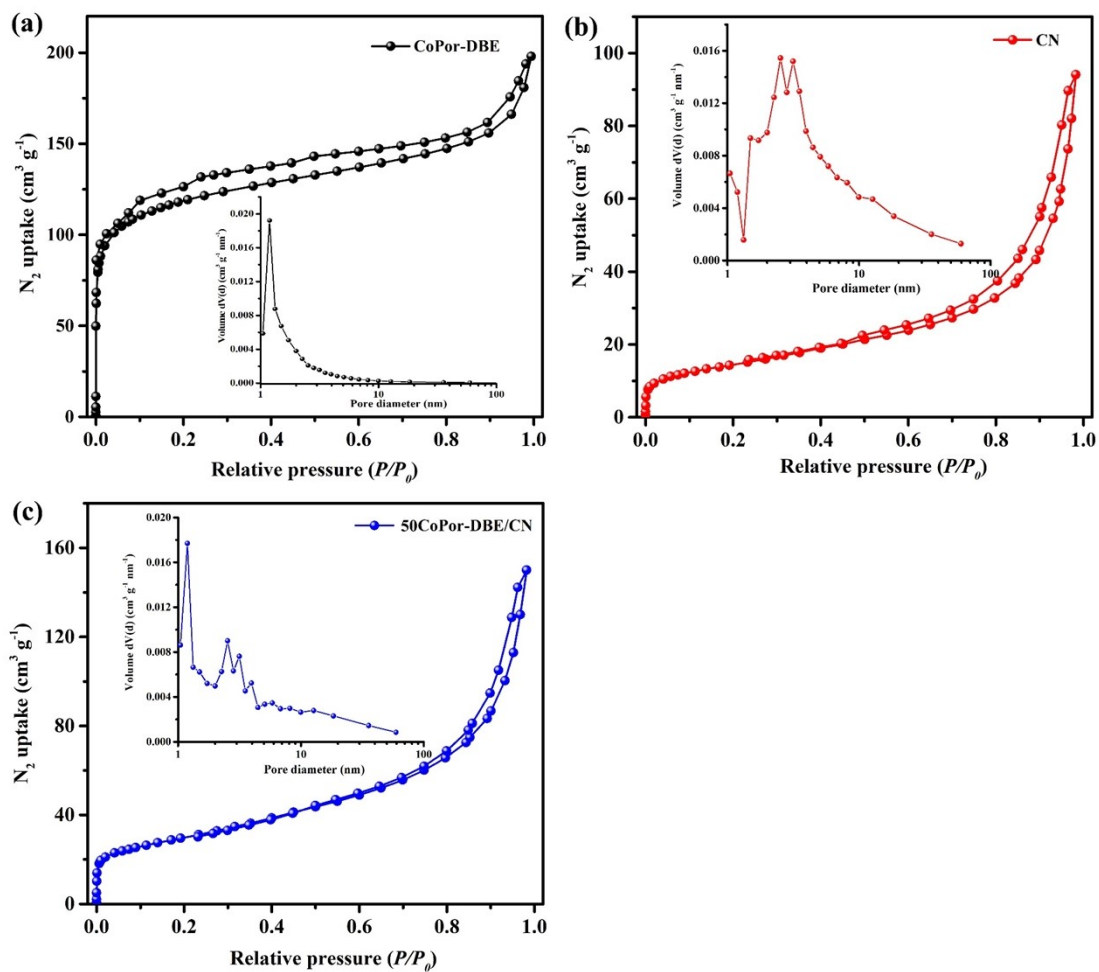


Fig. S5. N₂ adsorption-desorption isotherms (inset pore-size distribution profile) of (a) CoPor-DBE, (b) CN, and (c) 50CoPor-DBE/CN composite.

Table S1. The specific surface area and porosity of different samples.

Samples	S _{BET} (m ² /g)	Total pore volume (cm ³ g ⁻¹)
CoPor-DBE	442.34	0.2995
CN	51.49	0.1456
50CoPor-DBE/CN	105.83	0.2321

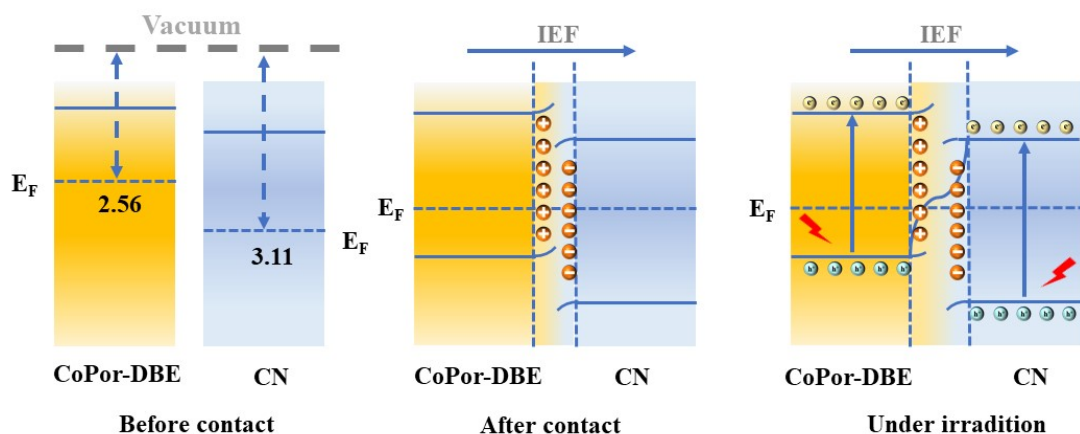


Fig. S6. Schematic diagram illustrating the S-scheme charge-transfer process in the CoPor-DBE/CN heterojunction.

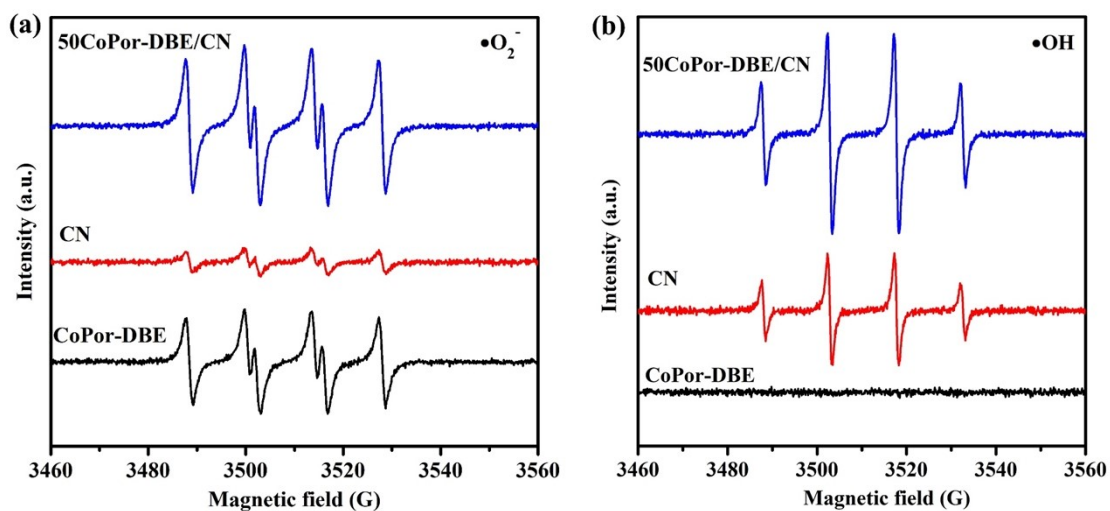


Fig. S7. DMPO spin-trapping ESR spectra recorded for (a) $\bullet\text{O}_2^-$ and (b) $\bullet\text{OH}$ over CoPor-DBE, CN, and 50CoPor-DBE/CN.

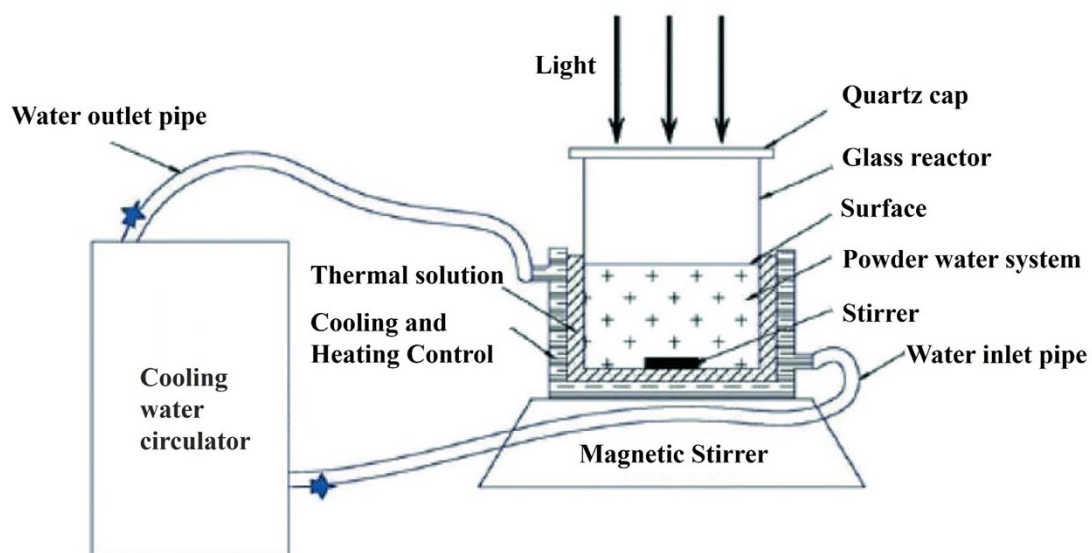


Fig. S8. Schematic diagrams of experimental setup for photocatalytic performance test.

Table S2. Comparison of the activity of 50CoPor-DBE/CN in the cooperative CO₂ reduction and tetracycline decomposition with the catalysts reported in literature.

Sample	Light source	TC degradation rate (%)	Yield (μmol g ⁻¹ h ⁻¹)	Ref.
SBNCN-3	300 W Xe lamp, (λ > 420 nm)	78	2.26	[1]
ZnO/CN	300 W Xe lamp	92.6	7.68	[2]
g-C ₃ N ₄ /BiOI	300 W Xe lamp, (λ ≥ 400 nm)	100	12.45	[3]
CuInZnS-Ti ₃ C ₂ T _x	300 W Xe lamp	98.5	10.2	[4]
Bi ₂ WO ₆ /BCDs	300 W Xe lamp, (λ > 420 nm)	80	12.1	[5]
Bi ₁₂ O ₁₇ Br ₂ /g-C ₃ N _{4-x}	300 W Xe lamp	97	11.2	[6]
50CoPor-DBE/CN	300 W Xe lamp (λ ≥ 400 nm)	93.8	16.7	This Work

Reference

- [1] Xu, Y.; You, Y.; Huang, H.; Guo, Y.; Zhang, Y. Bi₄NbO₈Cl {001} nanosheets coupled with g-C₃N₄ as 2D/2D heterojunction for photocatalytic degradation and CO₂ reduction. *J. Hazard. Mater.* **2020**, 381, 121159.
- [2] Pham, T. H.; Tran, M. H.; Chu, T. T. H.; Myung, Y.; Jung, S. H.; Mapari, M. G.; Taeyoung, K. Enhanced photodegradation of tetracycline in wastewater and conversion of CO₂ by solar light assisted ZnO/g-C₃N₄. *Environ. Res.* **2023**, 217, 114825.
- [3] Li, H.; Wang, D.; Miao, C.; Xia, F.; Wang, Y.; Wang, Y.; Liu, C.; Che, G. g-C₃N₄/BiOI S-scheme heterojunction: A 2D/2D model platform for visible-light-driven photocatalytic CO₂ reduction and pollutant degradation. *J. Environ. Chem. Eng.* **2022**, 10, 108201.
- [4] Wang, L.; Zhang, Z.; Guan, R.; Wu, D.; Shi, W.; Yu, L.; Li, P.; Wei, W.; Zhao, Z.; Sun, Z. Synergistic CO₂ reduction and tetracycline degradation by CuInZnS-Ti₃C₂T_x in one photoredox cycle. *Nano Res.* **2022**, 15, 8010-8018.

- [5] Li, X.; Yu, Y.; Wang, Y.; Di, Y.; Liu, J.; Li, D.; Wang, Y.; Zhu, Z.; Liu, H.; Wei, M. Withered magnolia-derived BCDs onto 3D flower-like Bi_2WO_6 for efficient photocatalytic TC degradation and CO_2 reduction. *J. Alloy. Compond.* **2023**, 965, 171520.
- [6] Jia, X.; Cao, J.; Sun, H.; Li, X.; Lin, H.; Chen, S. Interfacial engineering of $\text{Bi}_{12}\text{O}_{17}\text{Br}_2/\text{g-C}_3\text{N}_{4-x}$ S-scheme junction boosting charge transfer for cooperative tetracycline decomposition and CO_2 reduction. *Appl. Catal. B: Environ.* **2024**, 343, 123522.

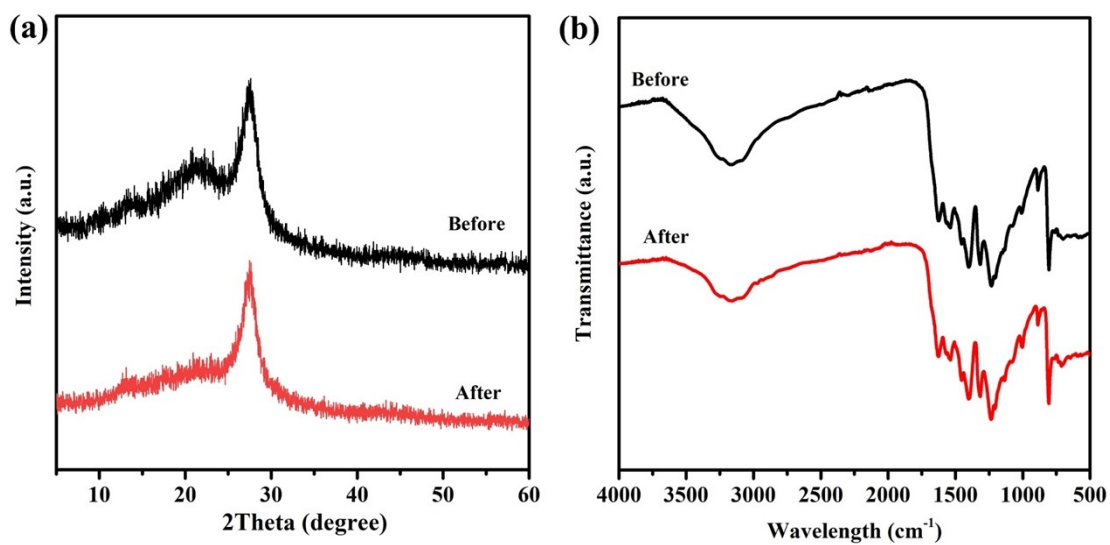


Fig. S7. (a) XRD pattern and (b) FT-IR spectra of 50CoPor-DBE/CN hybrid before and after cycling reaction.

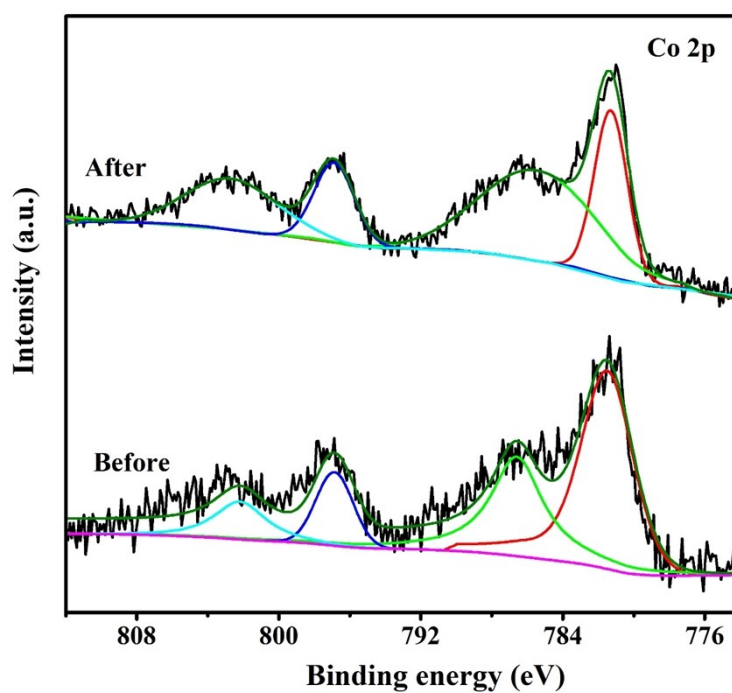


Fig. S10. High-resolution Co 2p spectra of CoPor-DBE/CN before and after cycling test.

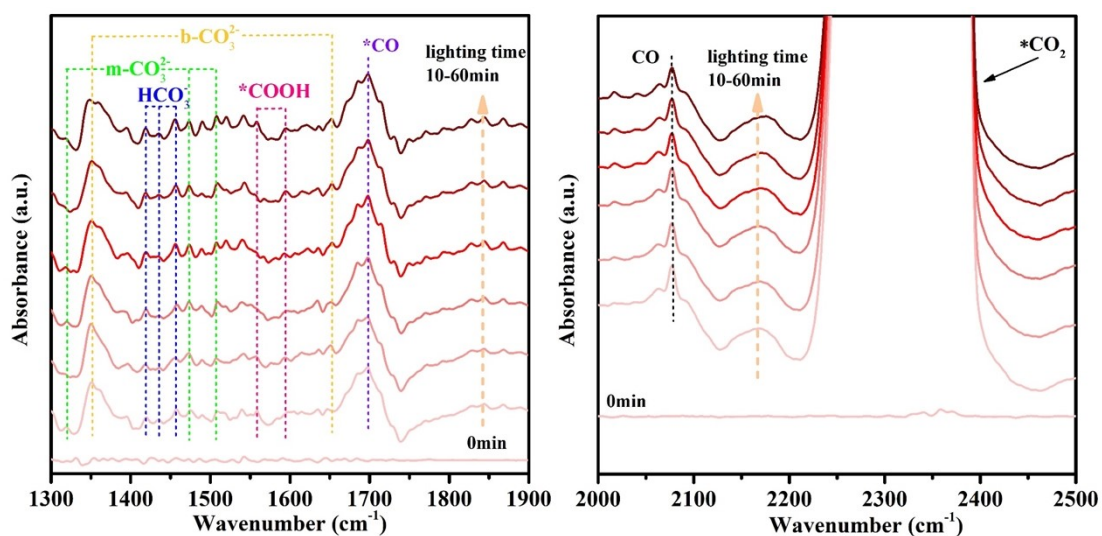


Fig. S11. In-situ FT-IR measurements for CO₂ photoreduction over 50CoPor-DBE/CN at room temperature under light irradiation.

Table S3. Fitted parameters from time-resolved PL spectra of pristine CN, CoPor-DBE and 50CoPor-DBE/CN.

samples	τ_1 (ns)	Rel. (%)	τ_2 (ns)	Rel. (%)	τ_{ave} (ns)
CN	0.75	39.72	7.35	60.28	4.72
CoPor-DBE	0.39	69.48	5.01	30.52	1.80
50CoPor-DBE/CN	1.82	31.29	9.85	68.71	7.34